

Synthesis and surface plasmon resonance of Au-ZnO Janus nanostructures

Jun Zhou(周俊), Jian-Shuo Zhang(张建烁), Guo-Yu Xian(冼国裕), Qi Qi(齐琦), Shang-Zhi Gu(顾尚志), Cheng-Min Shen(申承民), Zhao-Hua Cheng(成昭华), Sheng-Tai He(何声太), Hai-Tao Yang(杨海涛)

Citation: Chin. Phys. B . 2019, 28(8): 083301. **doi:** 10.1088/1674-1056/28/8/083301
Journal homepage: http://cpb.iphy.ac.cn; http://iopscience.iop.org/cpb

What follows is a list of articles you may be interested in

Measurement of transient Raman spectrum on gas-gun loading platform and its application in liquid silane

Yi-Gao Wang(汪贻高), Fu-Sheng Liu(刘福生), Qi-Jun Liu(刘其军), Wen-Peng Wang(王文鹏), Ming-Jian Zhang(张明建), Feng Xi(习锋), Ling-Cang Cai(蔡灵仓), Ning-Chao Zhang(张宁超)

Chin. Phys. B . 2017, 26(10): 103301. **doi:** 10.1088/1674-1056/26/10/103301

FDTD simulation study of size/gap and substrate-dependent SERS activity study of Au@SiO_2 nanoparticles

Jing-Liang Yang(杨晶亮), Ruo-Ping Li(李若平), Jun-He Han(韩俊鹤), Ming-Ju Huang(黄明举)

Chin. Phys. B . 2016, 25(8): 083301. **doi:** 10.1088/1674-1056/25/8/083301

Scattering of particles in wave beam based on series expansion

Li Ying-Le, Li Jin, Dong Qun-Feng, Wang Ming-Jun

Chin. Phys. B . 2014, 23(6): 063301. **doi:** 10.1088/1674-1056/23/6/063301

A polyene chain of canthaxanthin investigated by temperature-dependent resonance Raman spectra and density functional theory (DFT) calculations

Chen Yuan-Zheng, Li Shuo, Zhou Mi, Li Zuo-Wei, Sun Cheng-Lin

Chin. Phys. B . 2013, 22(8): 083301. **doi:** 10.1088/1674-1056/22/8/083301

Chiral asymmetry of anti-symmetric coordinates studied by the Raman differential bond polarizability of *S*-phenylethylamine

Shen Hong-Xia, Wu Guo-Zhen, Wang Pei-Jie

Chin. Phys. B . 2012, 21(12): 123301. **doi:** 10.1088/1674-1056/21/12/123301

Synthesis and surface plasmon resonance of Au–ZnO Janus nanostructures*

Jun Zhou(周俊)[1,2], Jian-Shuo Zhang(张建烁)[2], Guo-Yu Xian(冼国裕)[2], Qi Qi(齐琦)[2], Shang-Zhi Gu(顾尚志)[2], Cheng-Min Shen(申承民)[2], Zhao-Hua Cheng(成昭华)[2], Sheng-Tai He(何声太)[1,†], and Hai-Tao Yang(杨海涛)[2,‡]

[1] *School of Material Science and Engineering, Tianjin Polytechnic University, Tianjin* 300387, *China*
[2] *Beijing National Laboratory for Condensed Matter Physics, Institute of Physics, Chinese Academy of Sciences, Beijing* 100190, *China*

(Received 29 May 2019; revised manuscript received 11 June 2019; published online 9 July 2019)

Metal–semiconductor Janus nanostructures with asymmetry and directionality have recently aroused significant interest, both in fundamental light–matter interactions mechanism and in technological applications. Here we report the synthesis of different Au–ZnO Janus nanostructures via a facile one-pot colloid method. The growth mechanism is revealed by a series of designed synthesis experiments. The light absorption properties are determined by both the decrease of dipole oscillations of the free electrons and the plasmon-induced hot-electron transfer. Moreover, the finite-difference time-domain (FDTD) simulation method is used to elucidate the electric field distributions of these Janus nanostructures.

Keywords: Au–ZnO, SERS, finite-difference time-domain, mechanism

PACS: 33.20.Fb, 47.54.Bd, 47.54.Jk, 52.38.–r **DOI:** 10.1088/1674-1056/28/8/083301

1. Introduction

Metal–semiconductor heterogenous nanostructures have aroused significant interest, both in fundamental light–matter interaction mechanism and in technological applications (e.g., single-molecule detection, photocatalysis, and optoelectronic devices) because of their tunable properties by controlling the composition and unique morphology.[1–3] Among those heterogeneous nanostructures, Au–ZnO nanostructures are always an outstanding focus due to the fascinating light response effect from the strong surface plasmon resonance of Au and wide-band of ZnO. For example, the ultra-violet (UV) photo response of Au coated ZnO nanorods with a diameter of 100 nm has shown that the photosensitivity increases 10 times.[4] ZnO thin film incorporated with the Au nano-islands shows that both the PL and the photoconductivity increase by an order of magnitude.[5] Recently, the controlled design and preparation of colloidal Janus nanostructures have received considerable attention because they can greatly influence the chemical or physical properties due to the special asymmetry and directionality within a single unit.[6] Typically, Au–ZnO nanopyramids reported by Li *et al.* demonstrated better photocatalytic efficiency than pure ZnO nanocrystals.[7] Meanwhile, Au–ZnO nanoflowers reported by Peng *et al.* showed the higher catalytic efficiency than pure ZnO nanocrystals and other hybrid nanostructures for the photodegradation of rhodamine B.[8,9] Our previous work showed that each Au–ZnO nanoparticle with a break shell has enhanced optic absorption properties and an obvious SERS effect due to the plasma-induced hot electron transfer process.[10] At present, the major avenue toward bicomponent inorganic Janus nanostructures relies on the control of growth or the attachment of a second nanostructure onto a primary one via (i) heterogeneous nucleation, (ii) asymmetric modification at liquid/liquid interface, or (iii) non-epitaxial deposition on the surface of the first nanostructure and subsequent thermal dewetting into a single domain. The heterogeneous nucleation in organic solvent has become an effective and widely used method due to the as-prepared nanostructures with good crystallinity, monodispersity in size, and good control of the morphology. However, most of colloidal inorganic Janus nanostructures have been prepared by a tedious and time-consuming two-step growth method, with pre-synthesized seeds added.[11] The shape-controlled synthesis of the Janus nanostructures via a more facile way is still a challenge because of the complexity of the hybrid system and growth mechanism. Thus, a well-designed and controlled synthesis of Au–ZnO Janus nanostructures with diverse morphologies is of great importance, not only for developing a general method of preparing metal–semiconductor Janus nanostructures but also for investigating the structure–property–function mechanism.[12]

In this work, we prepare Au–ZnO Janus nanostructures with matchstick-like, branched, and dumbbell-like morpholo-

*Project supported by the National Natural Science Foundation of China (Grant Nos. 11274370 and 51471185) and the National Key Research and Development Program of China (Grant Nos. 2016YFJC020013 and 2018FYA0305800).

†Corresponding author. E-mail: sht-he@tjpu.edu.cn
‡Corresponding author. E-mail: htyang@iphy.ac.cn

© 2019 Chinese Physical Society and IOP Publishing Ltd

gies through a facile one-pot colloid synthesis method. The growth mechanism of the Au–ZnO Janus nanostructures is investigated by designing a serial of experiments with different reaction parameters. We explain the red-shift and broadening phenomena in the surface plasma resonance of different Janus nanostructures based on the Mie's theory and hot-electron transfer effect. Moreover, the electric field distributions of these Au–ZnO Janus nanostructures are investigated by finite-difference-time-domain (FDTD) simulations, which could benefit the studies of SERS enhancement mechanism. These results can greatly promote the application of functional metal–semiconductor Janus nanostructures by the controlled design of diverse asymmetry architectures.

2. Experiment

2.1. Materials and methods

Gold (III) chloride hydrate (99.99% trace metals basis, Beijing Chemical Factory), zinc acetate dihydrate (99.99% trace metals basis, Alfa Aesar), benzyl alcohol (99%, Alfa Aesar), octadecene (90%, Alfa Aesar), oleylamine (90%, Alfa Aesar), were straightly used without further purification prior to being used.

2.2. Synthesis of matchstick-like Au–ZnO Janus nanostructure

Matchstick-like Au–ZnO hybrid nanostructure was obtained by mixing 20-mg gold (III) chloride hydrate, 110-mg zinc acetate dihydrate, 4.18-g benzyl alcohol, 1.578-g octadecene, and 3-g oleylamine in a three-neck flask. Then, the mixture was heated to 120 °C slowly and kept at this temperature for a short time. The color of the mixture could change from yellow to brown. After that, the solution was further heated to 180 °C quickly and maintained at this temperature for 30 min. When the reaction was finished, the flask was cooled to room temperature naturally and the product was collected by centrifugation with ethanol and hexane. Finally, Au–ZnO Janus nanostructure was dissolved in hexane and stored at room temperature.

2.3. Synthesis of branched Au–ZnO Janus nanostructure

Branched Au–ZnO Janus nanostructure was synthesized under the similar conditions except for the adding of octadecene and the reaction temperature that was changed from 180 °C to 200 °C. The remaining procedures were exactly the same as those for synthesizing the matchstick-like nanostructure.

2.4. Synthesis of dumbbell-like Au–ZnO hybrid nanostructure

Dumbbell-like Au–ZnO Janus nanostructure was synthesized by changing the temperature from 180 °C to 160 °C. The other procedures were exactly the same as those for synthesizing the matchstick-like nanostructure.

2.5. Characterization

Powder x-ray diffraction (XRD) data were collected on a D2 PHASER x-ray diffractometer (Cu Kα radiation, $\lambda = 0.154$ nm) at 40 kV and 30 mA. The morphologies and structures of the samples were investigated by transmission electron microscopy (TEM, JEM-2100F with operation voltage 200 kV). UV-visible spectra were recorded with a Varian Cary 5000 ultraviolet-visible spectrophotometer.

3. Finite-difference time domain (FDTD) simulations

The FDTD simulations (Lumerical Solutions Ltd.) were carried out to elucidate the electric field distributions of Au–ZnO Janus nanostructures. The simulation zone consisted of periodic boundary conditions along the x, y, and z axes, and then perfectly matched layers (PML) were selected in the simulation zone to prevent the reflected electromagnetic waves from being reintroduced. A normal incident plane wave with a wavelength of 532 nm was used since it was the closest to the absorption peak of Au nanoparticles. To obtain accurate results and maximum field enhancement resolution, the mesh override region was set to be 2 nm, the size of Yee cell was 0.5 nm, the overall simulation time was 10000 fs which was long enough to ensure calculation convergence, and the geometric size was 300 nm$\times$300 nm$\times$300 nm. Furthermore, the surrounding medium was set to be air and the refractive index of ZnO was set to be 2.1.

4. Results and discussion

The synthesis of bicomponent Janus nanostructures requires an even higher degree of synthetic control than that of single-component nanostructures. To create bicomponent Janus nanostructures, it is crucial to suppress homogeneous nucleation of the second component as competitive reaction to heterogeneous nucleation on the preformed or in situ formed seeds. Thus, the ratio of seed to the second component precursor, and the adhesive Gibbs free energy at the interface between the seed and the overgrown particle are the key factors for the controlled synthesis of bicomponent Janus nanostructures.

Figure 1 shows the representative low-resolution TEM images of Au–ZnO Janus nanostructures with different precursor ratios of zinc acetate to gold chloride. Without Au precursors, ZnO nanostructures exhibit a shape like citrus chirocarpus and the longest side can achieve nearly 80.0 nm as shown in Fig. 1(a). After adding the Au precursors, the zinc acetate will process a heterogeneous nucleation on the surfaces of Au nanoparticles as seeds and form the well-dispersive matchstick-like Au–ZnO Janus nanostructure as show in Figs. 1(b)–1(d). All of the samples exhibit a uniform matchstick-like morphology consisting of single Au nanoparticles with a diameter of 8.0 nm. It should be noted that the diameter of Au nanoparticles is still around 8.0 nm when we keep the reaction for longer duration at different temperatures. This indicates that the concentration of Au precursors is low enough for the seeding growth. As the precursor ratios of zinc acetate to gold chloride decreasing from 3 to 1, the diameters of ZnO nanorods become smaller and the aspect ratio(length/diameter)increases from 1.9 to 5.1 gradually, while the sizes of Au nanoparticles are nearly the same. With the increase of the potion of Au precursor, the growth concentration of Zn ions around each Au seed decreases due to the increasing of the number of Au nanoparticles for the heterogeneous nucleation, which results in the fact that the ZnO nanorods have a prior growth direction because the thermal dynamics, other than the chemical dynamics, dominates the growth process.

Figure 2 shows the as-prepared Au–ZnO Janus nanostructures for different duration at 180 °C. When the duration is 15 min, 20 min, and 40 min, the average lengths of ZnO nanorods are 23.4 nm, 38.1 nm, and 38.7 nm, respectively. Correspondingly, the aspect ratios of ZnO nanorods are 3.1, to 3.8, and 4.9, respectively. It should be noted that the average length and aspect ratio of ZnO nanorods reach the maximum values of 46.0 nm and 5.1 in the duration of 30 min as shown in Fig. 1(d). This indicates that the atoms of ZnO at the end of nanorod may diffuse towards the center due to the long heating time after the Zn precursors have been exhausted about in 30 min.

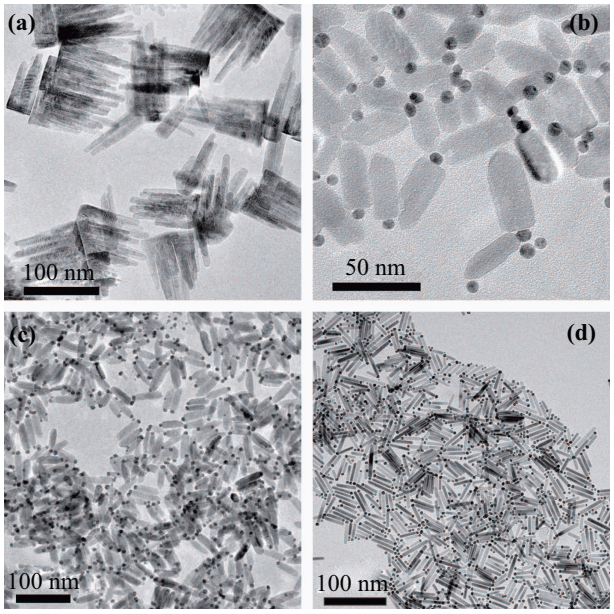


Fig. 1. Transmission electron microscopy (TEM) images of Au–ZnO Janus nanostructures prepared (a) without gold chloride and with different molar ratios of hydrate zinc acetate to gold chloride: (b) 3, (c) 2, and (d) 1.

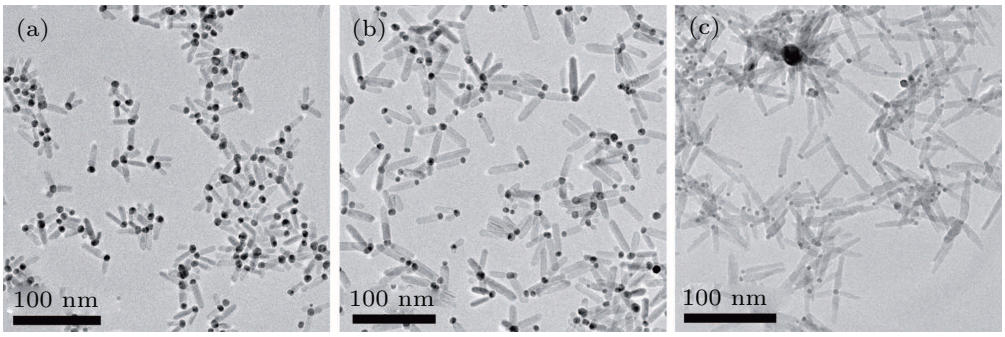


Fig. 2. TEM images of Au–ZnO Janus nanostructures prepared at 180 °C for different durations: (a) 15 min, (b) 20 min, and (c) 40 min.

Figure 3 shows the TEM images of Au–ZnO Janus nanostructures synthesized at the same reaction parameters except for different temperatures. When the temperature increases from 160 °C to 180 °C, the Janus nanostructure will change from dumbbell-like into matchstick-like nanostructure with a parallel self-assembly tendency due to a uniform morphology and a good dispersion. At 200 °C, branched Au–ZnO nanostructure is formed in which each one consists of a pure Au nanoparticle and two or three branched ZnO nanorods. Adjusting the temperature from 205 °C to 215 °C, the number of ZnO nanorods in branched nanostructures presents an increasing tendency as shown in the Figs. 3(e) and 3(f). The maximum number is five, which is popular in the case of 215 °C. Meanwhile, the average length of branched ZnO nanorods also increases with the reaction temperature increasing. The higher reaction temperature usually supplies higher adhesive Gibbs free energy at the interface of Au–ZnO Janus nanostructure, which allows the nucleation of Zn precursor on the multiple

crystalline planes of Au nanoparticles to grow up a complex branched Au–ZnO Janus nanostructure. Meanwhile, as a result of more nucleation sites and the insufficient number of Zn precursors, some insolated Au nanoparticles can be observed (as shown in Fig. 3(f)), although the molar mass values of all precursors and surfactants are the same as those at low temperatures.

Figure 4 shows the high resolution transmission electron microscope (HRTEM) images of dumbbell-like, matchstick-like, and branched Au–ZnO Janus nanostructure. The high resolution transmission electron microscope images indicate that the plane interspace of Au nanoparticles is 0.235 nm which belongs to the (111) plane while the lattice spacing of ZnO nanorods is 0.260 nm which belongs to the (101) plane of wurtzite-type ZnO. These results are well consistent with the d values calculated from the XRD patterns in Fig. 5(a). We can hardly tell any obvious lattice defects based on the high resolution transmission electron microscope images, which means that the qualities of all three kinds of Au–ZnO Janus nanoparticles are perfect.

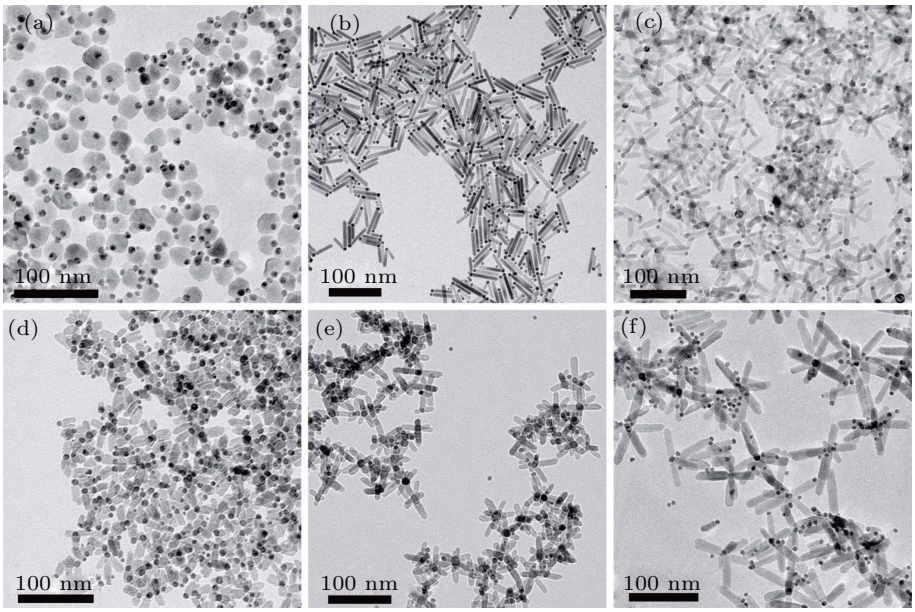


Fig. 3. TEM images of Au–ZnO Janus nanostructures prepared at different temperatures: (a) 160 °C, (b) 180 °C, (c) 200 °C, (d) 205 °C, (e) 210 °C, and (f) 215 °C.

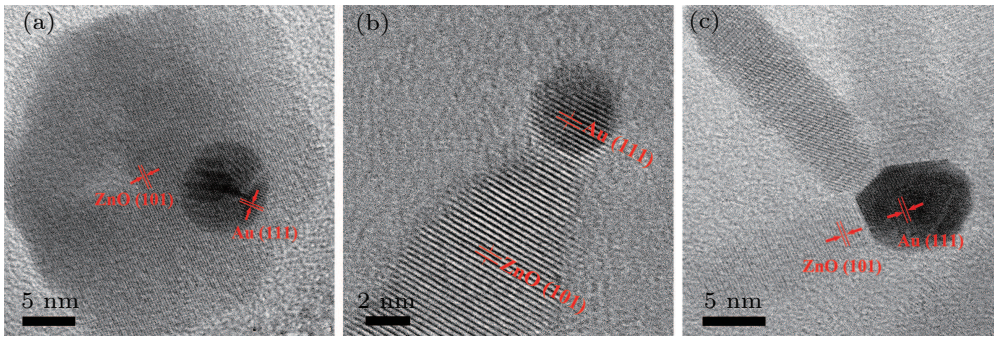


Fig. 4. High resolution transmission electron microscopy (HRTEM) images of different Au–ZnO Janus nanostructures: (a) dumbbell-like, (b) matchstick-like, and (c) branched.

Figure 5(b) shows the UV-vis spectra of different Au–ZnO Janus nanostructures with pure Au nanoparticles and ZnO nanorods. The pure Au nanoparticles exhibit a strong plasmon absorption at 520 nm that corresponds to its characteristic collectively oscillation frequency.[13] While the absorption peak in dumbbell-like Au–ZnO Janus nanostructure presents a red-shift from 520 nm to 538 nm, which arises from an overall increase of the refractive indices of the dielectric surroundings.[14] If the shape changes from the dumbbell-like into branched and matchstick-like nanostructure, then the plasmon absorptions present a continuous red-shift to 545 nm and 556 nm, respectively. According to the Mie theory, the red-shift of plasmon absorption is ascribed to the decrease of dipole oscillations of the free electrons when the effective local dielectric function around Au nanoparticles increases after the ZnO nanorods have been combined together. Meanwhile, the strong interface interaction in the Au–ZnO Janus nanostructure can lead the plasmon-induced hot electrons to transfer from Au nanoparticles into the valance band of ZnO nanostructure. The transfer causes the conduction band of ZnO to bend downwards, which results in a slightly red-shift of the

ground excitonic state of ZnO nanoparticles from 358 nm to 364 nm.[15] Also, the broadening cross-sections of the Au plasmon resonance absorption peaks results from the variation of electron density of Au nanoparticles due to the plasmon-induced hot-electron transfer within the Janus nanostructure. Therefore, the dielectric circumstances and hot-electron transfer have a large influence on the plasmon absorption for different Au–ZnO Janus nanostructures.[16]

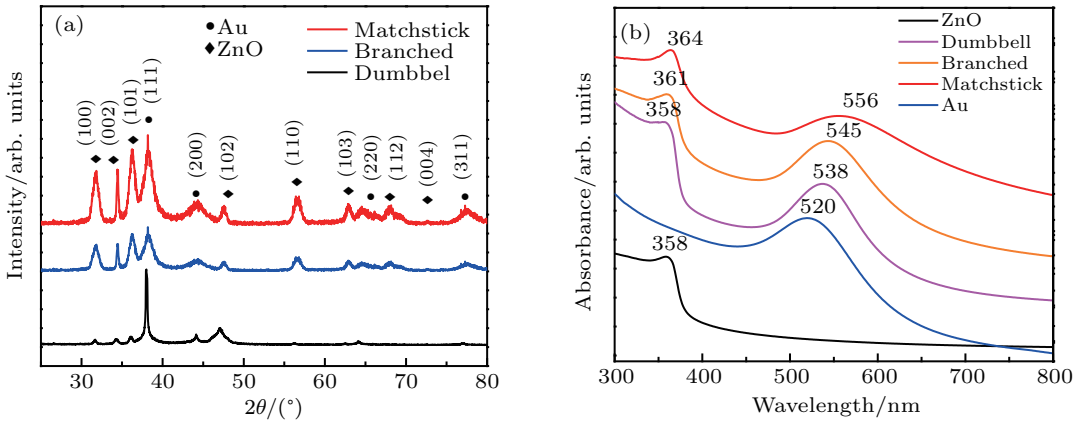


Fig. 5. (a) XRD patterns and (b) UV-vis spectra of different Au–ZnO Janus nanostructures.

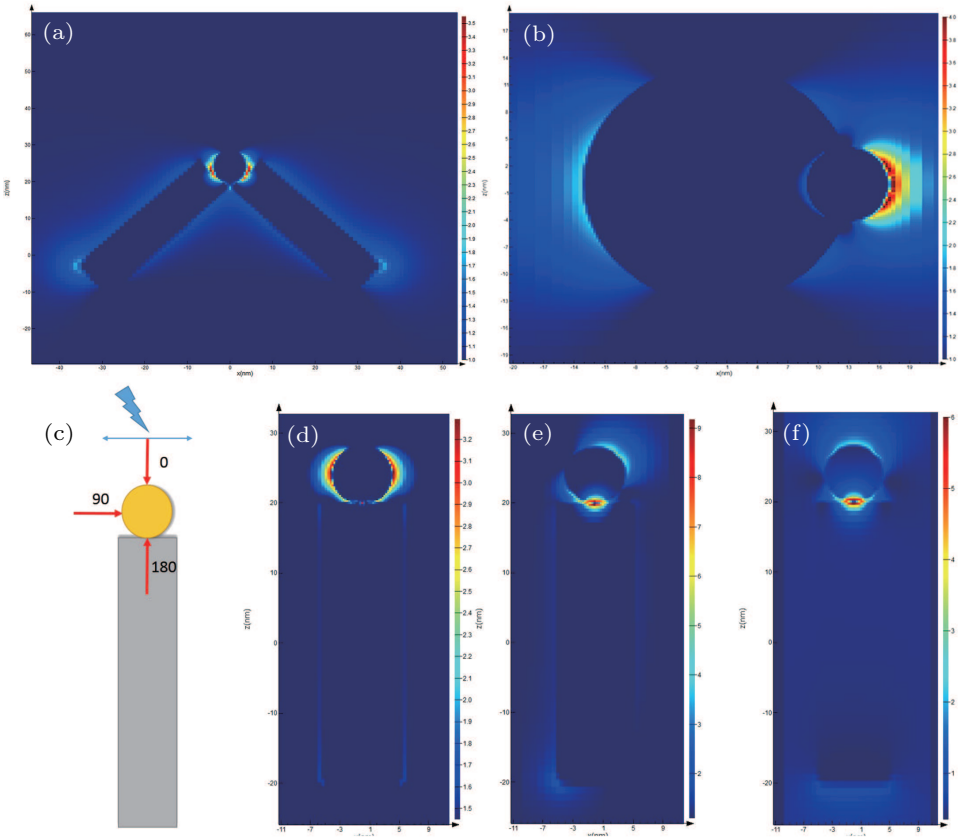


Fig. 6. Electric field distribution in FDTD simulations for (a) branched and (b) dumbbell-like Au–ZnO Janus nanostructure with incident angle of 0°; (c) model of the matchstick-like Au–ZnO nanostructure and electric field distribution at different angles of incident light: (d) 0°, (e) 45°, and (f) 90°.

The FDTD method is used to simulate the electromagnetic field distribution around the light-illuminated Au–ZnO Janus nanostructure by solving the Maxwell's equations.[17] Figure 6 shows the field distribution of matchstick-like, branched, and dumbbell-like Au–ZnO Janus nanostructures. When the Au–ZnO Janus nanostructures are excited by the 532-nm polarized light source, the Au nanoparticles can generate a strong plasmon excitation and electronic field.[18] However, such enhancements have a definite angle-dependent relationship. A distinct hot-spot occurs and exhibits the highest enhancement of the electric field intensity at an incident angle of 90° because of the strongest dipole oscillations of the free electrons. The enhancements at incident angles of 135° and 180° are exactly the same as those at 45° and 0°, respec-

tively. The hot-spots induced by the incident light provides an increasing number of hot-electrons at the interface between noble metal and semiconductor nanostructure.[19] Such hot-spots will result in a more effective transfer of hot electrons across the Schottky barrier to the conduction band of ZnO nanorod.[20,21] Some literature has reported that these hot-spots can greatly improve the efficiency of plasmon-enhanced photocatalytic water splitting by the enhancement of the local electric field.[22–24] Of the three structures, *i.e.*, matchstick-like, branched, and dumbbell-like Au–ZnO Janus nanostructure, the matchstick-like nanostructure has the biggest exposed surface of Au nanoparticles and the longest length of ZnO. The longer ZnO nanorods can provide a longer relaxation path of hot electrons and prevent the hot electrons from damping, which is beneficial for the improvement of transfer efficiency. Meanwhile, the larger surface of Au nanoparticles can generate stronger plasma resonance and more hot electrons entering the semiconductor, thus giving rise to the charge-transfer enhanced SERS effect and photocatalysis required donor electrons.

5. Conclusions

In this work, we propose a facile one-pot colloid method of synthesizing the matchstick-like, branched and dumbbell-like Au–ZnO Janus nanostructure through the successive nucleation of Au and ZnO precursors in a continuous heating process. The adhesive Gibbs free energy at the interface is a critical factor for the selective growth of ZnO nanostructures on the Au nanoparticles. Meanwhile, the Mie theory and hot-electron transfer are used to explain the red-shift and the broadening of absorption cross section in the light absorption properties in the UV-vis range. Moreover, we can observe that the electromagnetic fields in these Janus nanostructures exhibit some enhancements because the dielectric media around the noble metal have different morphologies and sizes. Therefore, our experimental results and theoretical simulations are expected to provide a new insight into the growth mechanism of Janus nanoparticles and inspire people to fully utilize these surface plasmon resonance in a variety of areas such as functional photoelectronic devices and highly sensitive SERS materials.

References

[1] Wang D S and Li Y D 2010 *J. Am. Chem. Soc.* **132** 6280
[2] Zhang J T, Tang Y, Lee K and Ouyang M 2010 *Nature* **466** 91
[3] Kwak J, Bae W K, Zorn M, Woo H, Yoon H, Lim J, Kang S W, Weber S, Butt H J, Zentel R, Lee S, Char K and Lee C 2009 *Adv. Mater.* **21** 5002
[4] Dixit T, Palani I A and Singh V 2016 *Mater. Lett.* **181** 183
[5] Wu S H, Chan C H, Chien C H, Yaseen M T, Liang C T and Chang Y C 2016 *Appl. Phys. Lett.* **108** 041104
[6] Walther A and Müller A H E 2013 *Chem. Rev.* **113** 5194
[7] Li P, Wei Z, Wu T, Peng Q and Li Y D 2011 *J. Am. Chem. Soc.* **133** 5660
[8] Chen Y Z, Zeng D Q, Zhang K, Lu A L, Wang L S and Peng D L 2014 *Nanoscale* **6** 874
[9] Zeng D Q, Gong P Y, Chen Y Z, Wang C G and Peng D L 2015 *Mater. Lett.* **161** 379
[10] Liu L P, Yang H T and Ren X 2015 *Nanoscale* **7** 5147
[11] Schladt T D, Shukoor M I, Schneider K, Tahir M N, Natalio F, Ament I, Becker J, Jochum F D, Weber, Khler S O, Theato P, Schreiber L M, Snnichsen C, Schrder H C, Muller W E G and Tremel W G 2010 *Angew. Chem. Int. Ed.* **49** 3976
[12] Wanga P L, Linc Z Y and Su X O 2017 *Nano Today* **12** 64
[13] Juste J P, Santos I P, Liz L M and Mulvaney P 2005 *Coordination Chemistry Reviews* **249** 1870
[14] Wu X F, Song H Y, Yoon J M, Yu Y T and Chen F Y 2009 *Langmuir* **25** 6438
[15] Lee M K, Kim T G, Kim W and Sung Y M 2008 *J. Phys. Chem. C* **112** 10079
[16] Ding W, Chen Y H and Li Z Y 2014 *Chin. Phys. B* **23** 037301
[17] Xie S X, Li H J, Zhou X, Xu H Q and Fu S L 2010 *Chin. Phys. B* **19** 077803
[18] Averitt R D, Sarkar D and Halas N J 1997 *Phys. Rev. Lett.* **78** 4217
[19] Alvarez-Puebla R, Liz-Marzán L M and García de Abajo F J 2010 *J. Phys. Chem. Lett.* **1** 2428
[20] Castillo A S, Hermo M C, Gonzalez B R, Lorenzo M P, Wang Z M, Kong X T, Govorov A O and Duarte M A C 2016 *J. Phys. Chem. C* **120** 11690
[21] Das S N, Choi J H, Kar J P, Moon K J, Lee T and Myounga J M 2010 *Appl. Phys. Lett.* **96** 092111
[22] Liu Z W, Hou W B, Pavaskar P, Aykol M and Cronin S B 2011 *Nano Lett.* **11** 1111
[23] Zhang P, Wang T and Gong J L 2015 *Adv. Mater.* **27** 5328
[24] Ingram D B and Linic S J 2011 *J. Am. Chem. Soc.* **133** 5202